Materials & Design 213 (2022) 110335

Contents lists available at ScienceDirect

Materials & Design

journal homepage: www.elsevier.com/locate/matdes

Understanding and designing post-build rolling for mitigation of residual stress and distortion in wire arc additively manufactured components

Valeriy Gornyakov, Jialuo Ding, Yongle Sun *, Stewart Williams

Welding Engineering and Laser Processing Centre, School of Aerospace, Transport and Manufacturing, Cranfield University, Cranfield MK43 0AL, UK

HIGHLIGHTS

- Post-build rolling can efficiently mitigate residual stress and distortion in wire arc additive manufacturing (WAAM).
- Influences of roller design, rolling load and friction coefficient on plastic strain and residual stress distributions are analysed and elucidated.
- Slotted roller can more effectively introduce tensile plastic strain and reduce the WAAM tensile residual stress than the flat and profiled rollers.
- Increase of rolling load improves efficacy of rolling process to reduce WAAM residual stress and distortion.

GRAPHICAL ABSTRACT

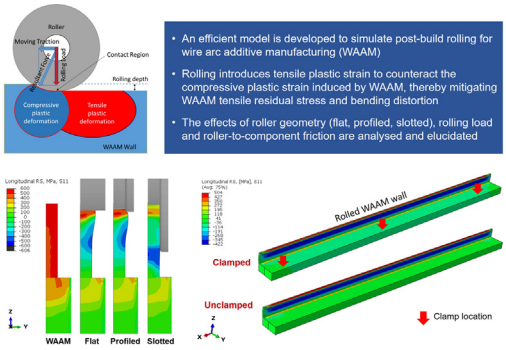

ARTICLE INFO

Article history:
Received 27 July 2021
Revised 29 November 2021
Accepted 19 December 2021
Available online 21 December 2021

Keywords:
Directed energy deposition
Cold working
Residual stress
Plastic deformation
Roller geometry
Rolling load

ABSTRACT

Post-build rolling can mitigate residual stress (RS) and distortion in large-scale components built by wire arc additive manufacturing (WAAM). In this study, based on numerical simulations that considered both WAAM deposition and vertical rolling, the mechanisms of rolling-enabled mitigation of RS and distortion in a WAAM-built steel wall are elucidated. The influences of process configuration and condition, such as roller design (flat, profiled and slotted rollers), rolling load (25–75 kN) and roller-to-wall friction coefficient (0–0.8) on the distributions of plastic strain (PS) and RS were investigated. It is found that the slotted roller is most effective to introduce tensile PS for counteracting the compressive PS generated by the WAAM deposition, thereby reducing the tensile RS in the clamped condition and the final distortion after removal of clamps. Higher rolling load increases the rolling-induced tensile PS, which leads to more extensive mitigation of the WAAM-generated tensile RS. The simulations also demonstrate that the friction coefficient significantly affects the PS and RS when the slotted roller is employed. However, the efficacy of the flat/profiled roller is insensitive to friction coefficient. This study could underpin the development of an optimal post-build rolling process for efficient mitigation of RS and distortion in WAAM components.

1. Introduction

Wire Arc Additive Manufacturing (WAAM) is an emerging near-net-shape manufacturing technology, which has gained increasing

* Corresponding author.
E-mail address: yongle.sun@cranfield.ac.uk (Y. Sun).

https://doi.org/10.1016/j.matdes.2021.110335
0264-1275/

popularity in aerospace, automotive, military, and petroleum industries [1]. WAAM allows building of components with various dimensions, from relatively simple walls [2] and cylindrical structures [3], to complex parts with variable deposit features [3]. Parts with medium geometric resolution and surface quality [4] have been built using steel [2,5], aluminium alloy [6], titanium alloy [7,8], nickel superalloy [9], tantalum [10] and tungsten [11]. This new technology is based on sequential deposition of metallic layers with a wire consumable, an arc heat source, and a robotic manipulator under precise computer control. The standard welding equipment and consumables, which are widely available in the market and can be adopted by WAAM, reduce build-up and operational cost of WAAM [12]. Design flexibility, reduced manufacturing time and low buy-to-fly ratio [12] make the WAAM process attractive for small batch manufacturing.

One of the main challenges in applying WAAM for building large-scale structures is to control residual stress (RS) and distortion. RS arises from "deformation mismatch" between different regions of the deposit and substrate upon uneven heating and cooling [13]. RS may cause build distortion as well as stress corrosion cracking and brittle fracture [14–16], which all can lead to failure of WAAM parts. Heat treatment is an effective method to relieve RS [17], which normally works through evenly heating the component, thereby introducing plastic deformation and relaxing RS. However, this method is expensive and difficult to apply to large components, and it could adversely affect mechanical properties.

High pressure rolling has been developed as a versatile and cheap technique for reducing RS in welds [18]. The early research on such a RS mitigation method was conducted in Russia by Kurkin et al. [19]. Post-weld rolling was found effective to reduce RS even in thick weld joints [20] and the effectiveness is proportional to the rolling load [18]. In the last decade high pressure rolling has been also widely implemented for controlling RS and distortion in WAAM.

Colegrove et al. [2] reported reduction of RS and distortion in WAAM steel components after inter-layer rolling with profiled (i.e., roller with radiused groove) and slotted rollers. The results demonstrated a trend that, as the rolling load increases (from 25 kN to 75 kN), the final distortion decreases for both inter-layer and post-build rolling. The slotted roller was found to be more effective in reducing RS and distortion. Interestingly, the distortion of the post-build rolled sample is comparable to that of the inter-layer rolled sample.

Colegrove et al. [21] and Martina et al. [7] investigated inter-layer rolling with flat and profiled rollers on WAAM Ti-6Al-4V components. For both types of rollers, the distortion decreased with the increase of the rolling load. However, the distortion cannot be completely eliminated, similar to the observation in WAAM steel components [2]. This can be partially attributed to the absence of side restraint during the rolling of the WAAM wall, which causes significant deformation in the transverse direction. For complicated structures, Hönnige et al. [22] investigated the effect of inter-layer rolling on intersections based on "inverted" roller (i.e., roller with convex surface), and reported that although the inverted roller can improve the microstructure, it does not affect RS distributions at the intersections, presumably because the thermal influence of WAAM deposition dominated over the rolling [22].

Most of the reported high-pressure rolling experiments for WAAM components were conducted between deposition of each layer (i.e., inter-layer rolling), which is time consuming and costly. Fortunately, as suggested by Colegrove et al. [2], the post-build rolling (i.e., rolling on the last layer only) can provide an efficacy similar to the inter-layer rolling for distortion reduction, with much less time consumed and cost incurred, while the efficacy of post-build rolling for residual stress mitigation has not been examined in experiments.

Finite Element Analysis (FEA) has been proved a robust method for studying manufacturing processes [33,34], which can significantly reduce experimental effort. The influences of rolling load and friction on RS distribution have been studied numerically by Cozzolino [24] for conventional welds and by Abbaszadeh et al. [25] for WAAM with inverted roller. Tangestani et al. [26] also investigated the effect of rolling using profiled and slotted rollers on the RS distribution in a WAAM wall. It was found that the increase in the rolling penetration led to a greater depth of compressive longitudinal RS in the wall.

However, neither of the rolling models by Abbaszadeh et al. [25] or Tangestani et al. [26] considered the initial PS generated by WAAM, which is an important variable and can affect strain hardening of the material during rolling and hence the model prediction accuracy. The influence of post-build rolling parameters on the WAAM-generated PS distribution and the mechanism of PS formation were not investigated in the literature, while PS distribution plays a key role in RS formation after rolling. Although the effects of the rolling parameters and roller design on RS distribution were demonstrated in the literature, the roles of different influential factors in the RS mitigation mechanism, and the RS redistribution after removal of clamps and the resultant distortion have not been revealed. For the slotted roller, the friction effect has not been investigated either. Therefore, the aim of this research is to fill the knowledge gap and to investigate the influences of the main process parameters of the post-build rolling on the mechanical response of the WAAM deposited wall to vertical rolling. The considered process-related variables include roller geometry, rolling load and friction coefficient, and the mechanical variables under investigation are PS, RS and distortion.

2. Material and methods

2.1. Material and experiments

The WAAM deposition and post-build rolling to be modelled are consistent with previous experiments [2]. A structural steel plate (grade S355JR-AR) with dimensions of 500 mm × 60 mm × 12 mm was used as the substrate (see chemical compositions in Table 1). Cold Metal Transfer process was used with Lincoln Electric SupraMIG G3Si1/ER70S-6 wire (⌀0.8 mm, see chemical compositions in Table 1). An approximately 490 mm long linear wall was built with a layer width of 5 mm and a layer height of 2 mm, and the deposition parameters are summarised in Table 2. The rolling loads ranged from 25 kN to 75 kN. Six clamps were applied during WAAM deposition and rolling, and the clamps were removed after manufacture.

2.2. Thermal-mechanical model of WAAM deposition

General purpose FEA software Abaqus was employed for the numerical simulations in this study. To obtain the PS and RS distributions caused by the WAAM deposition, an efficient thermal–mechanical model was employed, which has been validated using previous experimental data [27]. Firstly, the temperature field was predicted using a short multilayer thermal model with a calibrated double ellipsoidal heat source. Then the temperature solution was transferred to a short multilayer mechanical model, from which the PS and RS evolution during the deposition was calculated. The solution mapping method developed in Ref. [27] (Fig. 1) was used to transfer the steady-state solution of the short model to the full-size long model for determining final state after

Table 1
The chemical compositions of the substrate plate and the filler wire.

C, %	Mn, %	Si, %	P, %	S, %	N, %	Nb, %	Cu, %	Fe, %
The substrate steel grade S355JR-AR								
0.24	1.60	0.55	0.045	0.045	0.009	0.003–0.100		Balance
The filler wire Lincoln Electric SupraMIG G3Si1/ER70S-6								
0.08	1.50	0.92	⩽0.040	⩽0.035			0.16	Balance

Table 2
WAAM deposition parameters

Wire feed speed, m/min	Travel speed, mm/s	Heat input, J/mm	Assumed efficiency
10	8.33	269.5	0.9

removal of clamps, and it was also used to transfer the PS and RS solution obtained by the WAAM model to the short post-build rolling model for defining the initial condition before rolling. This modelling method is computationally efficient and applicable to both WAAM and rolling [27].

2.3. Post-build rolling model

Three sets of rolling models were developed to carry out parametric sensitivity analysis and furthermore to identify the RS and distortion mitigation mechanisms. In Set 1 models the effects of different rolling loads were studied for the flat roller without consideration of the WAAM process. The Set 2 models studied the effects of the friction coefficient on the PS and RS distributions for a given rolling load. Three different types of rollers, including flat, profiled, and slotted rollers, as shown in Fig. 2, were investigated. The Set 3 models focused on the investigation into the effects of rolling load and roller design on the PS and RS distributions. It should be noted that, the Set 1 models simulated the rolling alone, while the Set 2 and Set 3 models incorporated the PS and RS predicted by the thermal–mechanical WAAM model as the initial condition.

Table 3 summarises the different parameters used in the rolling models. For Set 2 models, four friction coefficients were considered, μ = 0; 0.1; 0.5; 0.8. A friction coefficient of 0.1 is recommended in the literature to simulate the lubricated contact between the roller and component [28–31], while the coefficient is assumed to be 0.5 for simulating the unlubricated steel-to-steel contact [23,32] and steel-to-aluminium contact [33,34]. For Set 3 models, it was assumed that μ = 0.1, as in the experiments lubricant was applied between the WAAM wall and the slotted roller [2].

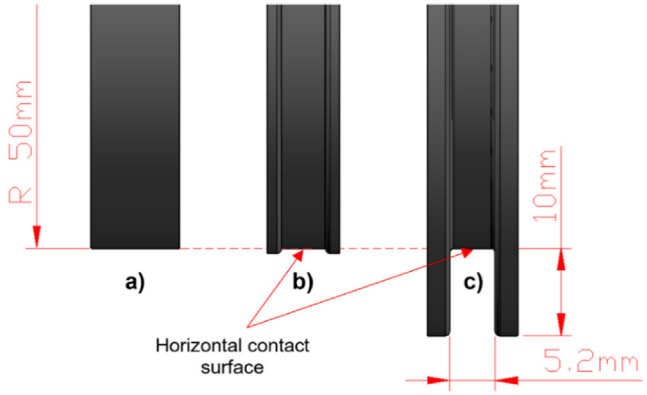

Fig. 2. Design of flat (a), profiled (b) and slotted (c) rollers.

Computationally efficient 3D short implicit transient model [35] was used in the numerical analysis. The thermal–mechanical model of WAAM deposition provides the initial condition for the rolling models (Sets 2 and 3) and the details of the WAAM model can be found in a previous paper by the same authors [27]. The rolling model consists of two components: the analytic rigid roller and the deformable WAAM wall bonded to the substrate (Fig. 3).

To simplify the geometry, the layer surface was assumed to be flat in the model. Flat layer is representative for small curvature

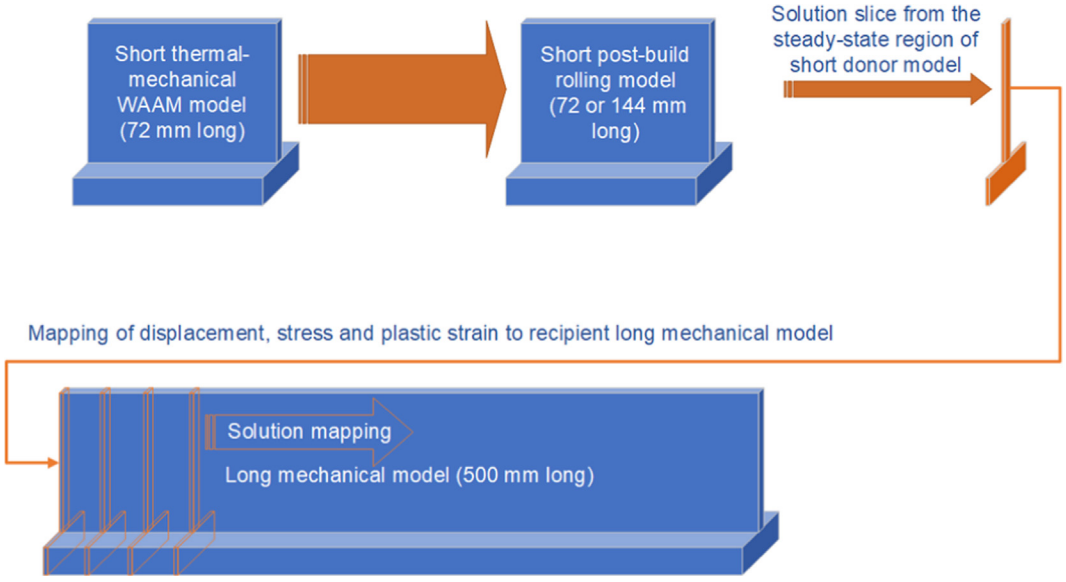

Fig. 1. Solution mapping method to transfer steady-state solution between different models [27].

Table 3
Rolling process variables considered in different sets of models.

	Roller Design	Rolling Load, F (kN)	Friction Coefficient, μ (–)	WAAM Deposition Before Rolling
Set 1*	Flat	25, 50, 75	0.5	Not included
Set 2	Flat	50	0, 0.1, 0.5, 0.8	Included
	Profiled	50	0, 0.1, 0.5, 0.8	Included
	Slotted	50	0, 0.1, 0.5, 0.8	Included
Set 3	Flat	25, 50, 75	0.1	Included
	Profiled	25, 50, 75	0.1	Included
	Slotted	25, 50, 75	0.1	Included

*These models are used to investigate the influence of the rolling alone on the material response.

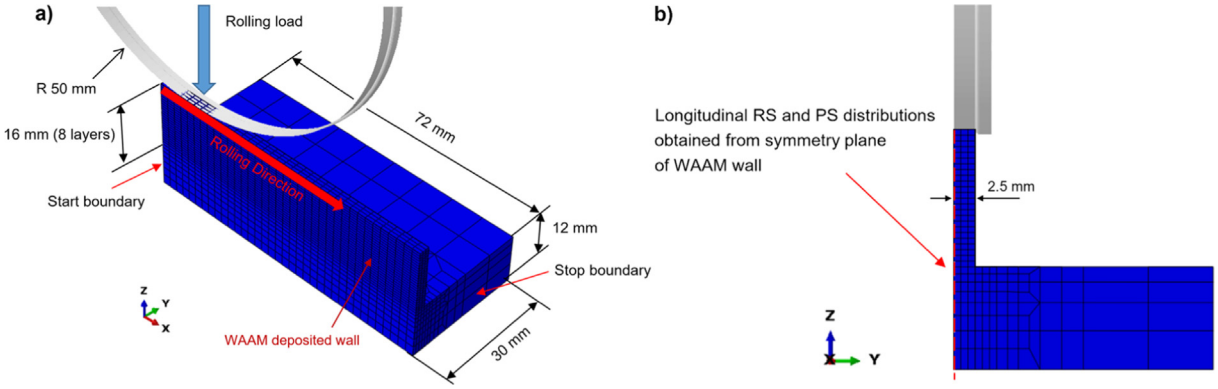

Fig. 3. Post-build rolling model for WAAM built wall using profiled roller: a) model dimensions, b) inspection plane. Note that only half component is considered due to symmetry.

bead, which is preferred in application of WAAM process to minimise surface roughness. The assumption of flat layer is widely used for WAAM simulations [13], and such assumption is also deemed acceptable for the high-pressure rolling model developed here to efficiently examine the effects of a wide range of rolling parameters. The assumption of flat horizontal contact surface (Fig. 2) is consistent with previous experiment using flat roller [7]. For the sake of comparison, same assumption is also adopted for the profiled and slotted rollers in the rolling model. Previous studies have investigated the effects of the roller surface curvature on the rolling model predictions. For instance, Abbaszadeh et al. [25] found that the surface radius of an inverted roller hardly affects the RS distribution, while the PS only slightly changes at a depth of 1–2 mm from the rolled surface. Similarly, Tangestani et al. [26] reported that the variation of curvature depth (associated with the profile radius) of the profiled roller has little effect on the longitudinal RS which is the major stress component concerned for WAAM.

In the short models with the flat and profiled rollers, the WAAM wall length is 72 mm, while for the slotted roller, the wall length is 144 mm because the slotted roller requires a longer distance to reach a steady state for the applied rolling loads. As demonstrated in Ref. [35], the deformable WAAM wall has sufficient length to attain steady-state rolling for the model to obtain an accurate and consistent solution. Further increase in wall length does not change the distribution of steady-state PS and RS.

The elastic–plastic properties of mild steel were used for the wall and substrate, as adopted from Ref. [36]. For simplification, it was assumed that the material properties are isotropic and not influenced by the microstructural changes caused by the thermal cycles and rolling. Previous measurements showed that the yield strengths of mild steel WAAM parts are similar in horizontal and vertical directions [37]. A yield strength value of 502 MPa was found in the certificate of ER70-S6 welding wire, which was used during experiments [2]. In addition, the previous experiments [2] showed that the longitudinal tensile RS reached 600 MPa on the border between the WAAM deposit and substrate. For mild steel, the magnitude of RS usually reached the yield strength [38,39]. These findings suggested that the actual yield strength of the WAAM deposit could be higher than the 390 MPa (room temperature) reported by Thompson et al. [36]. Therefore, the yield strength of the deposit was increased by 50 MPa in the rolling model compared to Thompson et al.'s data [36]. The material properties of the substrate were equivalent to those reported by Thompson et al. [36]. It should be noted that the Thompson et al.'s material data [36] contains detailed strain hardening information which is needed for the rolling simulations involving large plastic deformation.

The rolling model comprises two analysis steps: loading step and rolling step. In the loading step, the roller was gradually lowered via vertical load control until having pressed the top surface of the wall with the prescribed rolling load. The compressive loading location is 10 mm away from the *Start Boundary* (Fig. 3a). During the rolling step, the roller was moved horizontally along the wall length with the prescribed rolling load and at a horizontal speed of 3 mm/s. It should be noted that no torque was applied to the roller and the cylindrical roller was only allowed to rotate about the central axis. The rolling was terminated 12 mm away from the *Stop Boundary* (Fig. 3a). The marginal distance was chosen to prevent potential plastic collapse in the vertical direction at the edge of the wall due to the rolling load.

Surface-to-surface contact interaction with friction (penalty formulation) was specified between the surfaces of the roller and the wall. To simulate the clamping of the WAAM component to the worktable during the rolling process, the bottom of the substrate was constrained in all directions, which is similar to the method adopted by Abbaszadeh et al. [25]. To avoid the unrealistic longitudinal deformation due to reduced length in the short model, the *Start* and *Stop* boundaries of the short model were constrained for nodal movement in X direction (i.e., longitudinal rolling direc-

tion), and under such a boundary condition the steady-state solution of the short model is most close to that of the conventional full-size model [27].

The 3D 8-node linear brick elements with reduced integration (Abaqus designation C3D8R) were used in the mechanical model. A coarse mesh (element dimensions: 8 mm × 7.5 mm × 1.765 m m) was used for the substrate, while a fine mesh (element dimensions: 2 mm × 0.833 mm × 0.667 mm) was used for the deposited wall that was subjected to large deformation under rolling. A mesh sensitivity analysis was carried out to ensure that the results of the simulation are independent of the mesh density.

2.4. Long mechanical model

To determine the final PS and RS distributions and the distortion in the 500 mm long post-build rolled WAAM component after removal of the clamps, the solution mapping method [27] (Fig. 1) was employed. The solution slice from the steady-state region of the short post-build rolling model was spatially repeatedly mapped to the long mechanical model. The long model has the same cross-section, material properties and mesh density as the short model, but the length of the WAAM component in the long model is 500 mm, which is consistent with previous experiments [2].

2.5. Inspection planes

Detailed analysis was performed for an inspection plane located 48 mm away from the Start Boundary of the 72 mm long WAAM wall rolled by the flat/profiled roller and 86 mm away for the 144 mm long wall rolled by the slotted roller, as shown in Fig. 3b. This is the region where the rolling reached the steady state [35]. For the short models, all the inspections were performed for the simulations under the clamped condition. In the 500 mm long mechanical model the inspection data was collected in the mid-length plane, under both clamped and unclamped conditions.

2.6. Model computation time

A computer with four nodes was used for the computation. The maximum wall-clock time to obtain the solution of the 72 mm long WAAM wall model with the flat roller was 13 min 40 sec, while the 144 mm long model with the slotted roller consumed 1 h 13 min. The wall-clock time to solve the long mechanical model was 6 min 43 sec. Much more computational time is expected if a full-size model is used for the WAAM deposition and rolling simulations [27 35].

3. Results and discussion

Fig. 4 and Fig. 5 show the PS and RS distributions, respectively, after the WAAM deposition and the rolling using the flat, profiled and slotted rollers with a rolling load of 50 kN. The thermal cycles during the WAAM deposition caused significant compressive longitudinal PS, which is approximately −0.003 in the wall and −0.002 in the substrate immediately underneath the wall. The rolling induced tensile PS in the deposit and reduced the magnitude of compressive PS both in the wall and the substrate below the wall. Overall, the slotted roller induced larger magnitude of tensile PS in the wall, and it less markedly reduced the wall height, as compared to the flat and profiled rollers. Longitudinal tensile RS was generated in the wall after the thermal deposition cycles, and finally it was converted to compressive RS in the core of the wall by the rolling. The magnitude of the tensile RS in the substrate below the wall was also reduced by the rolling. Tensile RS remained in the region immediately under the rolled surface. Compared to the flat and profiled rollers, the slotted roller converted the tensile RS to compressive RS in more extensive region further away from the rolled surface.

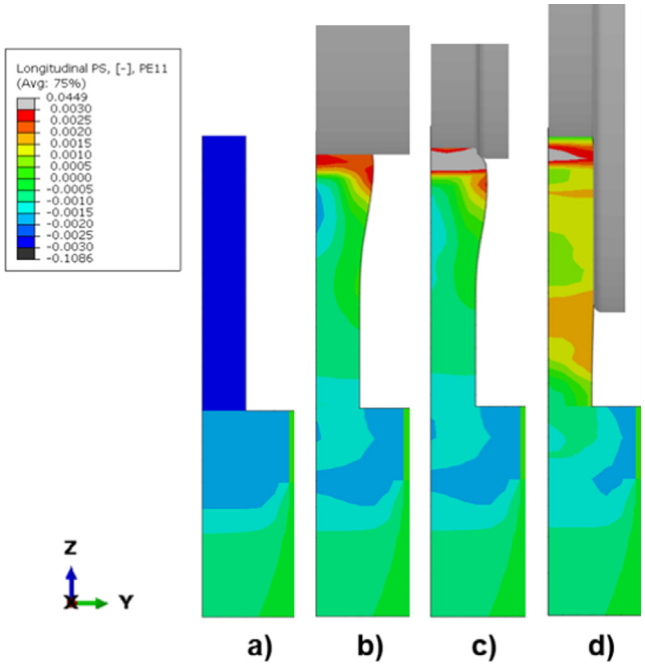

Fig. 4. Longitudinal PS distributions a) after WAAM deposition without rolling, and after rolling with b) flat roller, c) profiled roller and d) slotted roller at F = 50 kN and μ = 0.1.

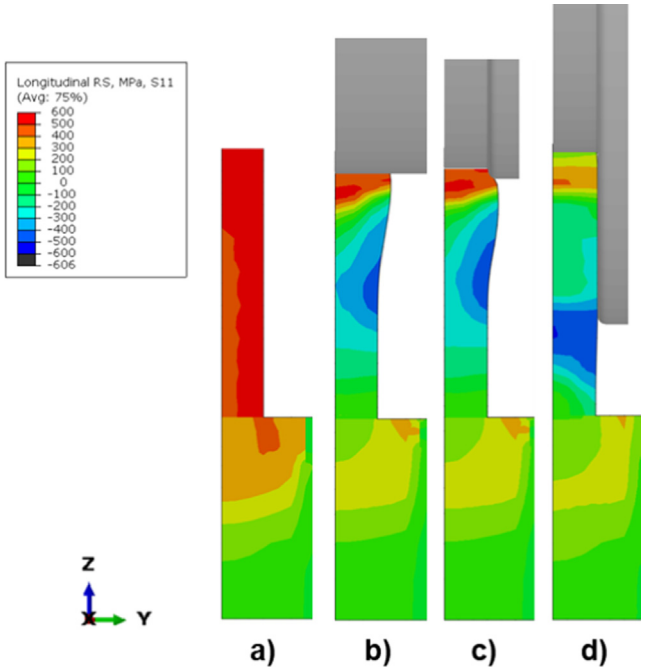

Fig. 5. Longitudinal RS distributions a) after WAAM deposition without rolling, and after rolling with b) flat roller, c) profiled roller and d) slotted roller at F = 50 kN and μ = 0.1.

3.1. Model Set 1

3.1.1. Longitudinal plastic strain formation during rolling

The mechanism of the PS generation in the wall during rolling with the flat roller is revealed in Fig. 6. To isolate the rolling effect,

the initial condition was assumed stress-free without considering WAAM deposition. During the loading step vertical compressive plastic deformation under the roller was generated, accompanying transverse and longitudinal tensile plastic deformation. Here the longitudinal PS is focused since the resultant longitudinal RS has highest magnitude. Considering longitudinal deformation, three plastically deformed zones can be identified under the roller (Fig. 6). Zone 1 and Zone 3 were deformed in compression, while Zone 2 was in tension. During the rolling step, the material in front of the roller experienced compressive plastic deformation (Zone 1), while the material behind the roller experienced tensile plastic deformation (Zone 2), which is due to the longitudinal stretching effect of the rolling (i.e., vertical compression and horizontal motion of the roller caused longitudinal elongation in Zone 2). Fig. 7 schematically shows the vertical rolling load and the horizontal moving traction, as well as the resultant plastic deformation zones. At the end of the rolling step, Zone 2 accounts for the major volume of the rolled wall.

3.1.2. Longitudinal stress evolution during rolling

The evolution of the longitudinal stress generated by the rolling with the flat roller is shown in Fig. 8. The plastic deformation induced by the rolling (Fig. 6) was constrained by the underlying material and then caused elastic straining between the unevenly deformed regions of the wall, resulting in the formation of RS. Four zones are defined to characterise the longitudinal stress evolution during the rolling process, i.e., Zone 1 in front of the roller below the wall surface, Zone 2 at the contact surface between the roller and wall, Zone 3 beneath the roller in the core of the wall and Zone 4 behind the roller near the rolled surface. In the end of the loading step (Fig. 8a), plastic deformation developed under the roller (Fig. 6a), giving rise to compressive stress in Zones 1, 2 and 3. During the rolling step, the compressively stressed zones (Zones 1, 2 and 3) followed the motion of the roller and extended gradually. A tensile RS zone (Zone 4) behind the roller developed due to the nonuniform distribution of plastic deformation (Fig. 6).

In the final state of the rolling, compressive RS is distributed in the core of the wall, while tensile RS is distributed near the rolled surface. The compressive plastic deformation concentrated near the stop boundary (Zone 1, Fig. 6c) is primarily responsible for

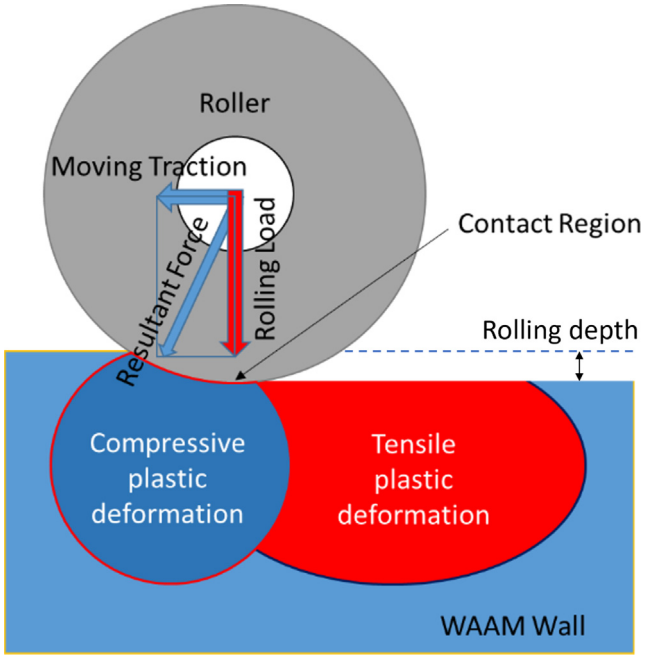

Fig. 7. Schematic of the acting forces during rolling with flat roller and the resultant longitudinal plastic deformation zones.

the tensile RS near the rolled surface, although tensile plastic deformation was generated near the rolled surface (Fig. 6c). Similar tensile RS near the rolled surface was also observed experimentally in WAAM parts [7,40] and found in previous rolling simulations for conventional welds [24]. However, the core of the wall was dominated by the effect of tensile plastic strain (Fig. 6c) and hence compressive stress was generated (Fig. 8c, d).

3.2. Model Set 2

3.2.1. Influence of friction coefficient

3.2.1.1. Longitudinal plastic strain. Fig. 9 shows the influence of the friction coefficient (i.e., friction between the wall and the roller) on

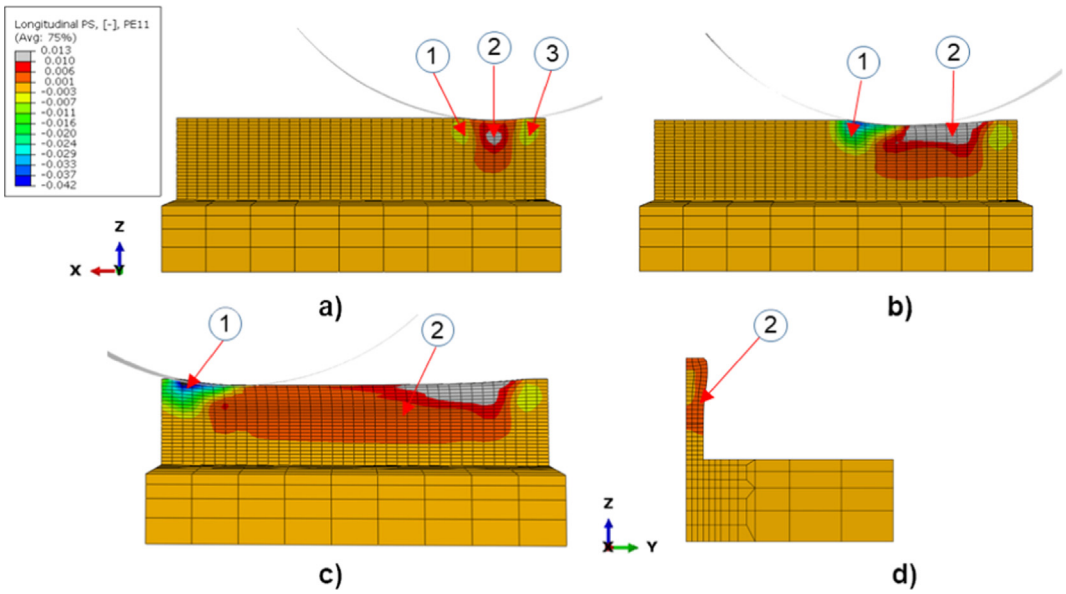

Fig. 6. Longitudinal PS generation during rolling with the flat roller (F = 50 kN and μ = 0.5): a) at the end of the establishment of contact in the loading step, b) at the beginning of the roller motion, c) at the end of the rolling step, and d) in the final rolling state on the transverse inspection plane. Note that in this analysis case the wall is assumed to be free from any strain and stress before rolling.

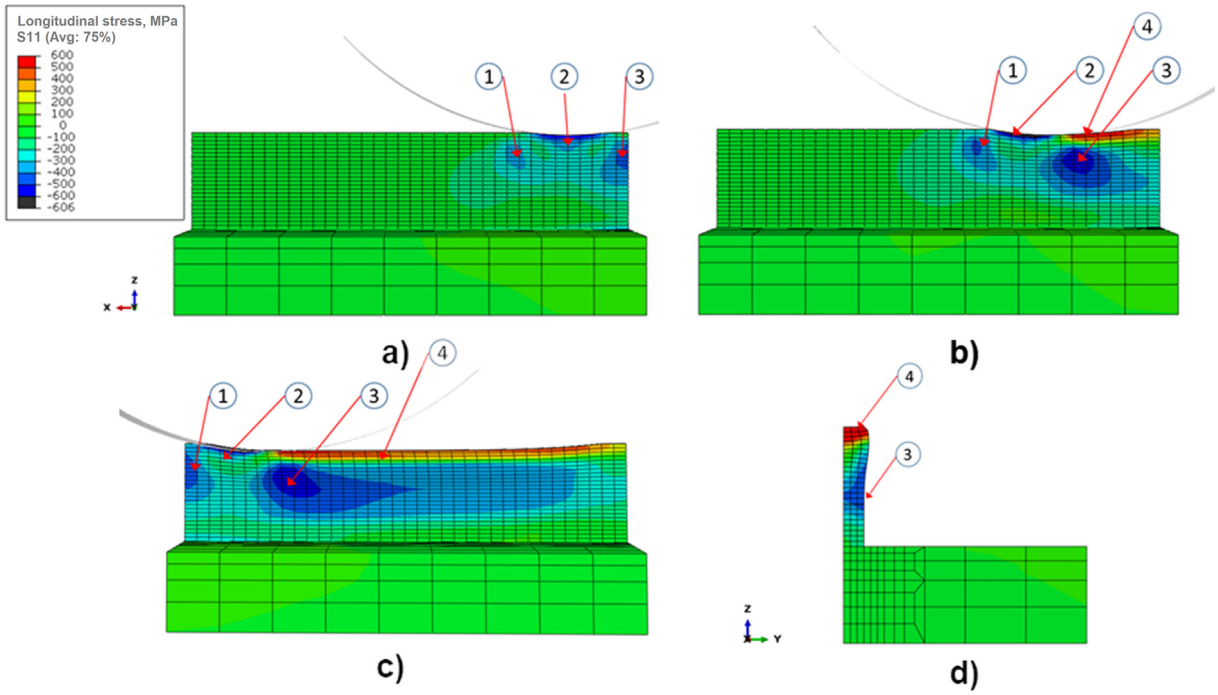

Fig. 8. Longitudinal stress evolution during rolling with flat roller (F = 50 kN and μ = 0.5): a) at the end of the establishment of contact in the loading step, b) at the beginning of the roller motion, c) at the end of the rolling step, d) in the final rolling state on the transverse inspection plane. Note that in this analysis case the wall and substrate are assumed free from any strain and stress before rolling.

PS distributions in the WAAM deposited wall after rolling with the flat, profiled and slotted rollers. Larger friction coefficient mainly caused increase of tensile PS under the rolled surface and such an effect is most marked for the slotted roller. Stronger friction enhanced the adhesion of the wall material to the surface of the roller, leading to greater tensile deformation near the rolled surface. The deformation constraint by the friction also contributes to the peak tensile PS 1–2 mm below the rolled surface. This effect limited the deformation of the contact surface but caused greater deformation underneath. Similar phenomenon has also been found in previous studies of rolling on single layer deposit [24], cylindrical samples [41], as well as weld seams [23,42] and WAAM wall [43].

For the slotted roller model with consideration of friction, the compressive PS due to the WAAM deposition was converted to tensile PS in the entire wall and the compressive PS in the substrate was significantly reduced (Fig. 9c). With the increase of friction coefficient, the rolling-induced tensile PS increased, and more material was affected through the depth of the wall. Friction also promoted deeper penetration of the slotted roller (Fig. 10), resulting in greater longitudinal tensile deformation. However, in the flat and profiled rollers models, the change of friction coefficient only caused small variation of the penetration. The additional friction between the wall side surface and the slot surface is responsible for the deeper penetration of the slotted roller. The lateral expansion of the wall during rolling enhanced the contact interaction, and the material adhered to the slot surface helped the roller plunge deeper into the wall. The larger the friction coefficient, the more significant the aforementioned effect.

3.2.1.2. Longitudinal residual stress. Fig. 11 demonstrates the influence of friction coefficient on the longitudinal RS distributions in the WAAM component rolled with flat, profiled and slotted rollers. Friction coefficient has a significant impact on the longitudinal RS distributions in the wall rolled by the slotted roller. The slotted roller with $\mu \geq 0.5$ converted the WAAM tensile RS to compressive RS in the whole wall. The main reason for this is the deeper penetration of the slotted roller into the wall and the stronger material adhesion for larger friction coefficients (Fig. 10). The increased penetration and the constraint of lateral deformation by the slot promoted larger longitudinal tensile deformation (Fig. 9c) and compressive RS (Fig. 11c). The compressive RS in the component can improve fatigue performance [44,45], while tensile RS has detrimental effects [45]. However, the friction effect on RS is insignificant for the flat and profiled rollers (Fig. 11a and b). Abbaszadeh et al. [25] also demonstrated that the variation of the friction coefficient between the inverted roller and the wall marginally affected the RS distributions at relatively low rolling loads.

The horizontal reaction force of the flat and profiled rollers is also insensitive to the friction. For F = 50 kN the horizontal force fluctuated in the range of 5–6 kN for both assumed friction coefficients of 0 and 0.8, implying that the horizontal resistance is mainly due to the indentation step created by the flat/profiled roller (Fig. 7) rather than the friction force.

The present modelling results suggest that rolling using a slotted roller with $\mu \geq 0.5$ could significantly improve the RS mitigation effectiveness of the rolling. However, in practice rolling using a slotted roller without application of lubricant was unsuccessful, since the slotted roller could be stuck to the WAAM wall due to insufficient horizontal moving capacity of the rolling rig. The simulation confirmed that for the slotted roller at F = 50 kN, the predicted horizontal reaction force on the pivot of the roller increased from 5.7 kN to 11 kN when the friction coefficient increased from 0.1 to 0.8. Practical implementation of the unlubricated post-build rolling with slotted roller should be tested using a rolling rig with larger moving capacity.

3.3. Model Set 3

3.3.1. Influence of rolling load

3.3.1.1. Longitudinal plastic strain. The effects of the rolling load on the WAAM-induced longitudinal PS for the flat, profiled and slotted

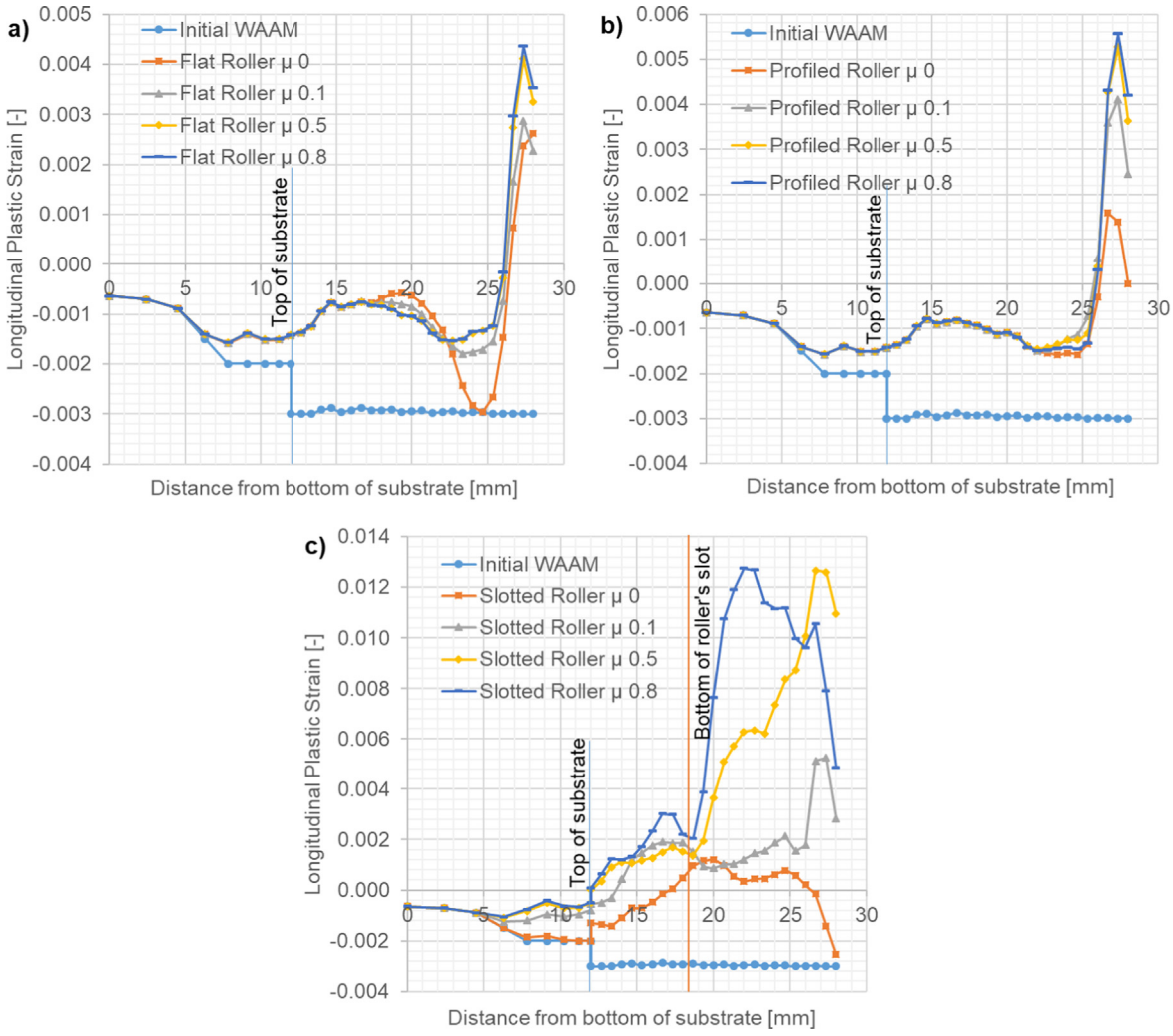

Fig. 9. Influence of friction coefficient on longitudinal PS in the WAAM built component after rolling: a) flat roller, b) profiled roller, and c) slotted roller (F = 50 kN).

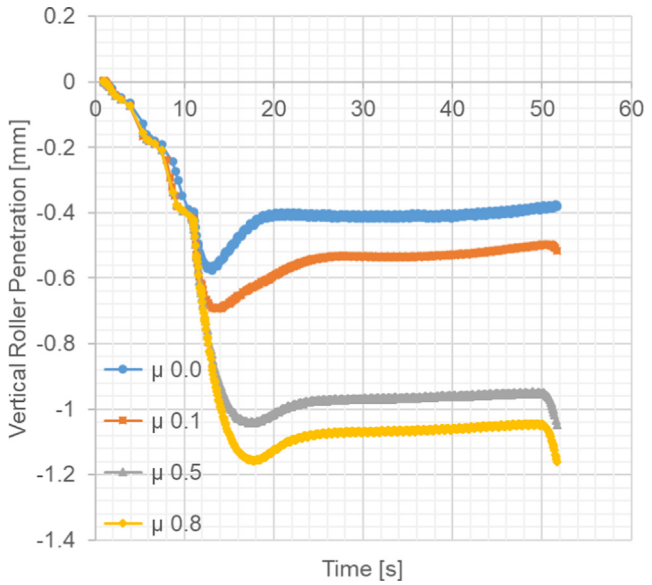

Fig. 10. Vertical penetration of slotted roller for different friction coefficients (F = 50 kN).

rollers are presented in Fig. 12 and Fig. 13. The compressive PS generated by the WAAM deposition can be significantly reduced by the rolling even with a relatively low rolling load of 25 kN. When a higher rolling load was used, the compressive PS in the wall transformed into tensile PS, and more significant plastic deformation occurred underneath the rolled surface. However, the higher rolling load of the flat roller led to undesirable larger reduction in wall height (Fig. 12), meaning that more material and WAAM deposition is needed to achieve the designed height.

With increase of the rolling load, the flat and profiled rollers models demonstrated a similar response. After rolling at F = 25 kN, the compressive PS reduced in the wall, as shown in Fig. 13 a) and b). As the rolling load increased to 50 kN, the compressive PS in the substrate reduced as well, and tensile PS was generated underneath the rolled surface. When the rolling load further increased to 75 kN, the compressive PS was further reduced in the wall and substrate, and the tensile PS under the rolled surface significantly increased. The peak PS is found to be 2 mm below the rolled surface, which can be enhanced by the friction as well (Section 3.2.1). Similar effect is also found for the slotted roller, except that the rolling with the slotted roller is more effective to reduce compressive PS and promote tensile PS in the wall.

3.3.1.2. Longitudinal residual stress. The effects of rolling load on the longitudinal RS induced by the WAAM deposition are presented in

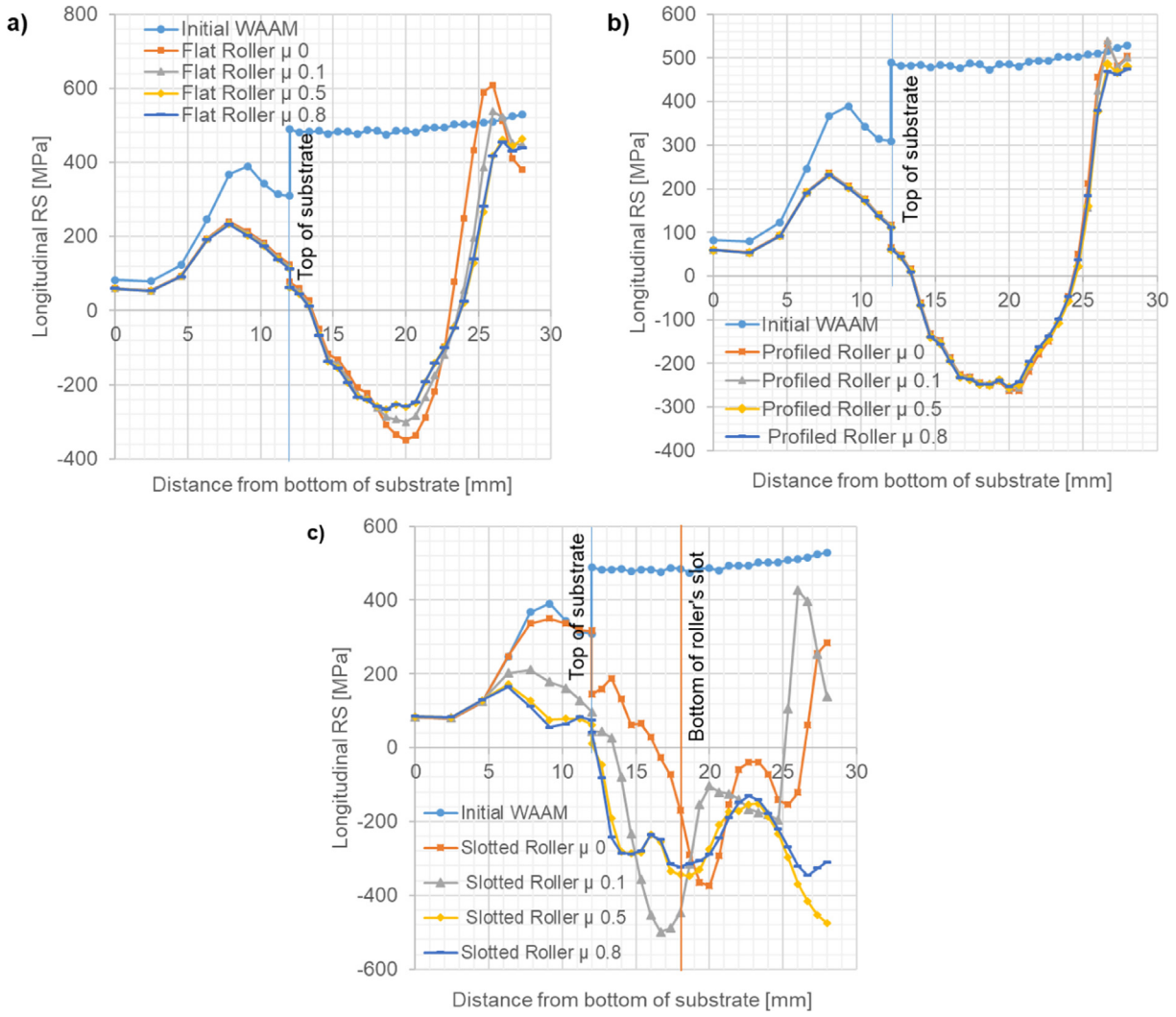

Fig. 11. Influence of friction coefficient on longitudinal RS distributions in the WAAM built component after rolling with a) flat roller, b) profiled roller and c) slotted roller (F = 50 kN).

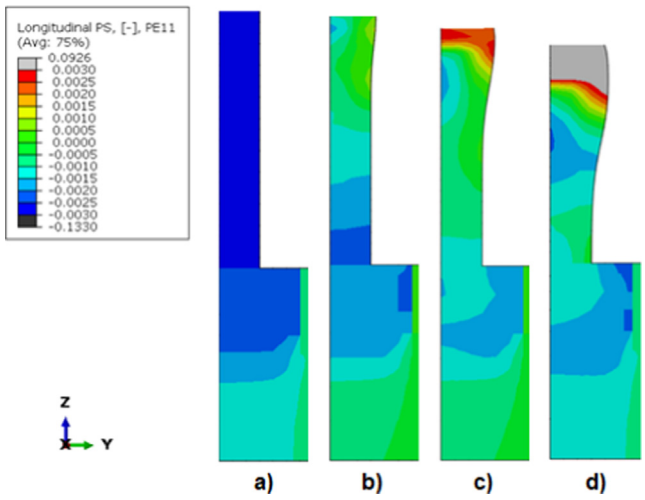

Fig. 12. Contour maps of longitudinal PS distributions in WAAM component a) after deposition without rolling, and after rolling with flat roller at rolling loads of b) 25 kN, c) 50 kN and d) 75 kN (μ = 0.1).

Fig. 14 and Fig. 15. The efficacy of the rolling to mitigate the WAAM-induced tensile RS is enhanced by increasing the rolling load for all the rollers. The WAAM tensile RS was converted to compressive RS in the central region of the wall, while the tensile RS near/in the substrate was reduced. With increase of rolling load, the peak of compressive RS increased and moved to a greater distance away from the rolled surface. This response can be explained by the greater effect of the compressively stressed Zone 3 (Fig. 8), which became larger and moved deeper due to the higher rolling load. In the flat and profiled rollers models, a higher rolling load caused an increase of tensile RS immediately under the rolled surface. It is also interesting to see that the rolling dominated the final RS and eliminated the feature of the WAAM deposition RS in the wall when the rolling load reached 75 kN.

In general, all the rolling models showed that as the rolling load increased, the tensile RS mitigation efficacy was enhanced, and compressive RS covered more extensive region in the wall. Therefore, from this perspective it is desirable to use the maximum rolling load to reduce tensile RS. However, an excessive rolling load could face practical difficulty regarding machine capacity and cause undesirable reduction of wall height (Fig. 14d). Moreover, it may not be always beneficial to reduce distortion (Section 4.3.4).

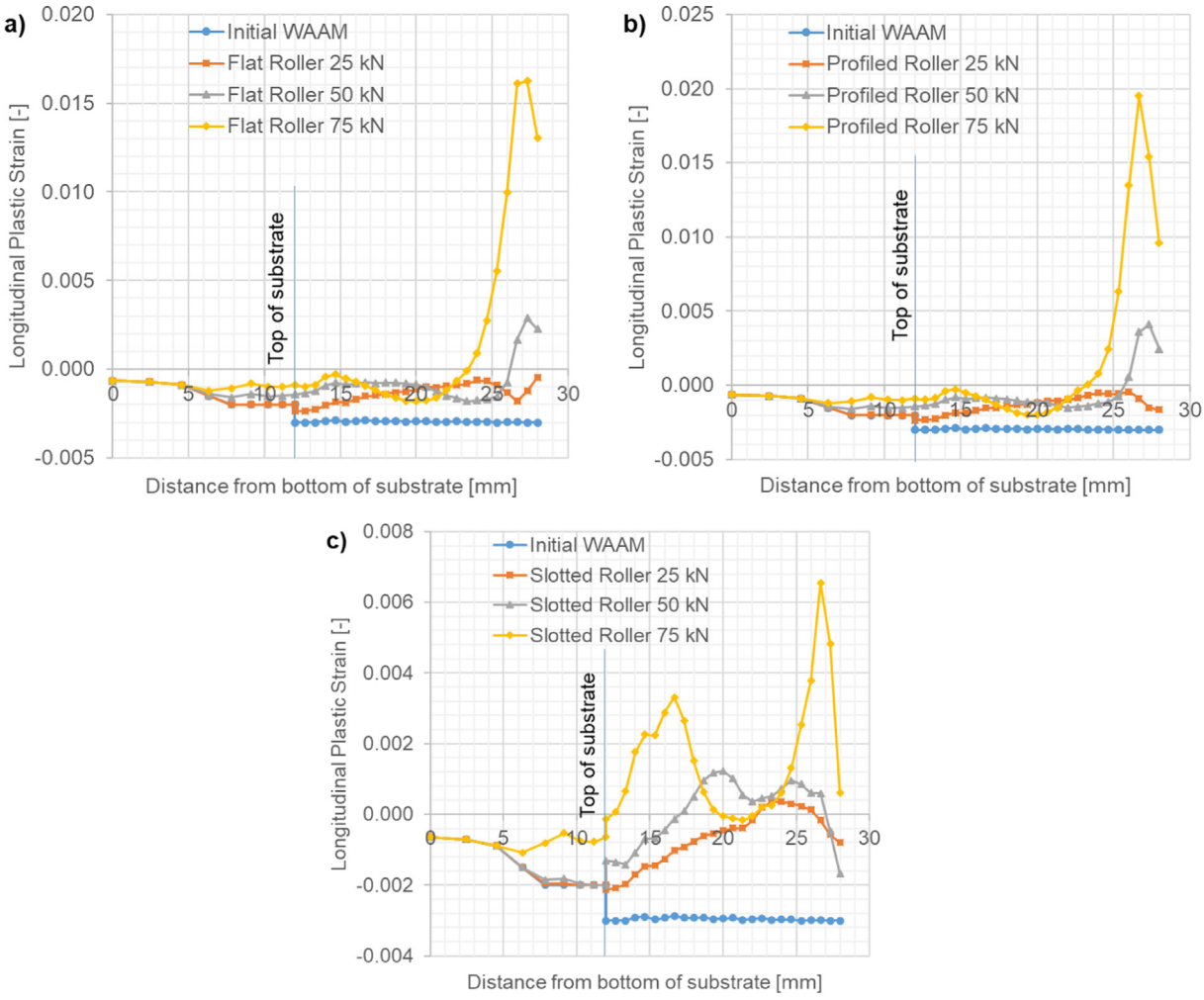

Fig. 13. Influence of rolling load on longitudinal PS in the WAAM component after rolling: a) flat roller, b) profiled roller, and c) slotted roller (μ = 0.1).

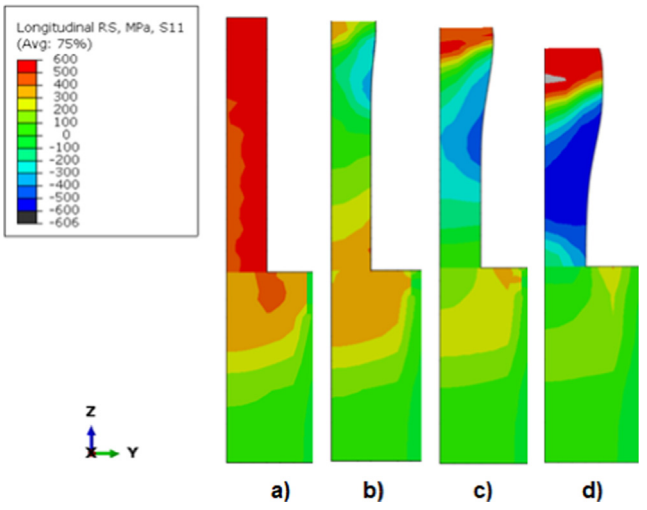

Fig. 14. Contour maps of longitudinal RS distributions in WAAM component a) after deposition without rolling, and after rolling with flat roller at rolling loads of b) 25 kN, c) 50 kN and d) 75 kN (μ = 0.1).

3.3.2. Influence of roller design

3.3.2.1. Longitudinal plastic strain. The effects of rolling on the WAAM-induced longitudinal compressive PS for different rollers are presented in Fig. 16. The flat and profiled rollers models had similar predictions for all the tested loads, despite that the profiled roller induced slightly larger longitudinal PS near the rolled surface, as compared to the flat roller. This difference arises because the lateral constraint provided by the edge of the profiled roller is larger than that solely provided by the friction for the flat roller, and hence the transverse deformation on the rolled surface can be more markedly constrained by the profiled roller. Similar behaviour was also observed in experiments by Martina et al. [7], who measured the average engineering strain induced by the profiled roller and found it was larger in the normal direction than in the transverse direction. But for the flat roller the transverse strain was larger than the normal strain. However, the flat and profiled rollers models predicted a similar PS distribution when the friction coefficient was 0.5 and higher, as shown in Fig. 9 a) and b).

Compared with the flat and profiled rollers, for all the rolling loads the slotted roller more extensively converted the compressive PS to tensile PS in the core of the wall. This is due to the more extensive constraining effect of the slot, which prevented large transverse expansion and promoted the longitudinal deformation. In contrast, the flat and profiled rollers produced greater magnitude of tensile PS mainly in the region that is 3–5 mm below the rolled surface.

3.3.2.2. Longitudinal residual stress. Fig. 17 shows the influence of roller design on the longitudinal tensile RS generated by the

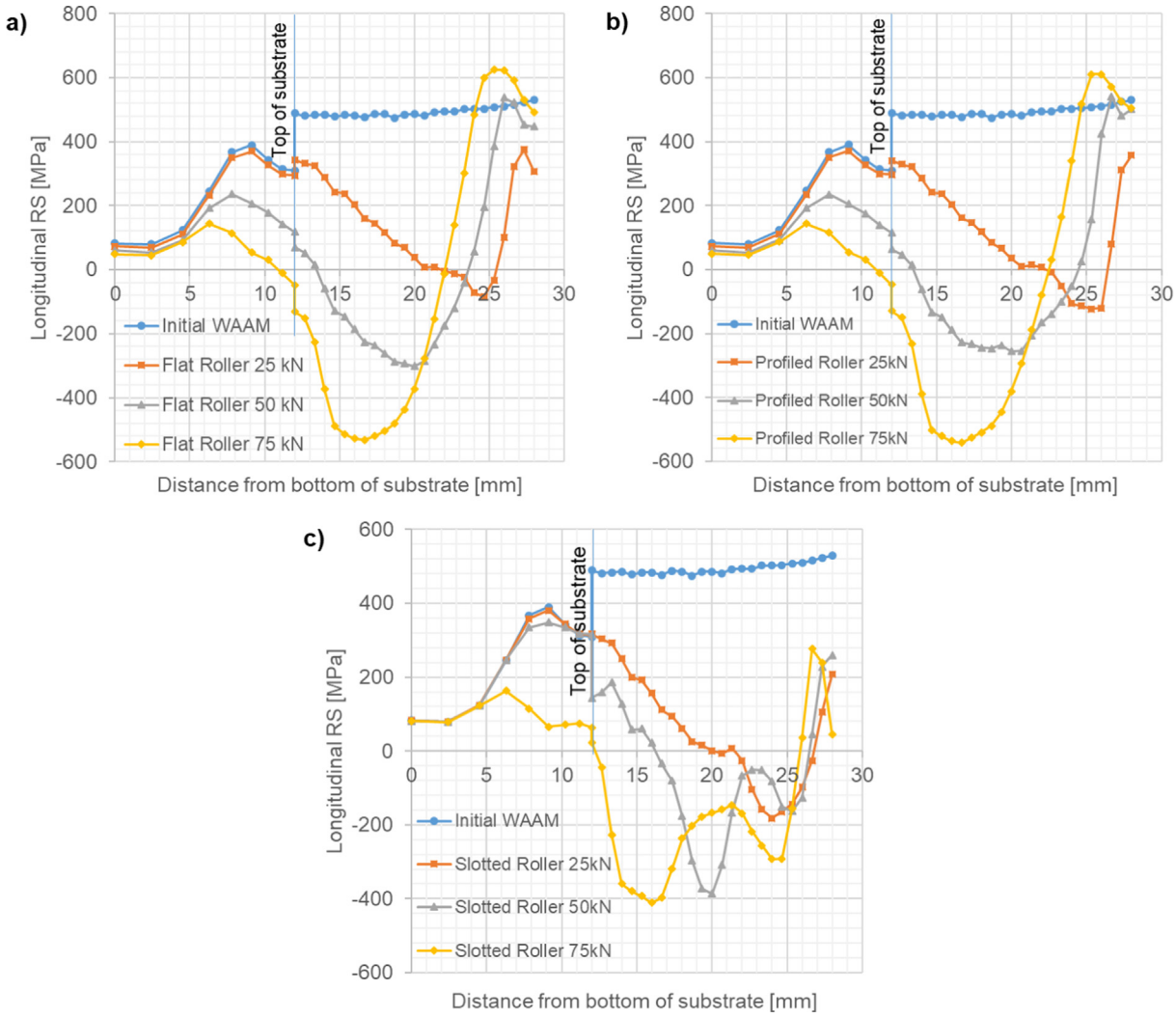

Fig. 15. Influence of rolling load on the longitudinal RS in the WAAM component after rolling: a) flat roller, b) profiled roller, and c) slotted roller (μ = 0.1).

WAAM deposition. The predicted RS distributions are compared between the rolling with the flat, profiled and slotted rollers. Under all the considered rolling loads, the flat and profiled rollers demonstrated similar RS distributions with minor difference in the region immediately under the rolled surface. In contrast, the slotted roller reduced the WAAM tensile RS more effectively and led to relatively uniform compressive RS distribution in the core of the wall at F = 75 kN. The main reason for such a stress feature is that the slot surface constrained the transverse deformation and meanwhile promoted the longitudinal deformation.

The design of roller has a great impact on the final PS and RS after rolling and thus determines the effectiveness of the post-build rolling. For all the considered rolling loads, compared to the flat and profiled rollers, the slotted roller induced more extensive tensile PS and the compressive RS region is deeper in the wall. In other words, the reduction in tensile RS by the slotted roller was found in a larger volume in the wall. Based on the results of this study, it is recommended that post-build rolling with a slotted roller should be further developed for minimising RS in steel WAAM structures.

3.4. PS and RS distributions and distortion in large-scale post-build rolled WAAM component

To investigate the PS and RS distributions and distortion in the large-scale WAAM component, the steady-state solution obtained from the short rolling model was transferred to the long mechanical model using the solution mapping method [27] (Fig. 1). Fig. 18 shows the RS distribution and the deformed configuration in the rolled full-length WAAM component before and after removal of clamps. Two narrow tensile zones are formed on the top and bottom of the wall, between which there is a wide compression zone. The distortion is barely seen, implying that the rolled wall is free from distortion issue. By contrast, significant bending distortion was observed in the as-built WAAM component [27].

Fig. 19 presents the effect of the post-build rolling on the WAAM-generated longitudinal RS distribution along the wall height, as predicted by the long mechanical model before and after removal of clamps. High tensile RS in the as-built WAAM wall was balanced by the reaction force at the clamps. The removal of clamps caused significant redistribution of tensile RS in the wall and the contiguous substrate. As the wall shrank after removal of clamps, the tensile RS relaxed and reduced markedly, and even converted to compressive RS at the top of the wall. The clamps removal in the model of WAAM + Rolling caused minor redistribution of longitudinal RS. The RS distribution remained virtually same as that before the clamps removal. This can be attributed to the dominant influence of rolling on RS at the 50 kN rolling load. As the tensile RS in the wall was already largely mitigated by the rolling under the clamped condition, the total vertical reaction force at the three clamps for the half model was reduced from

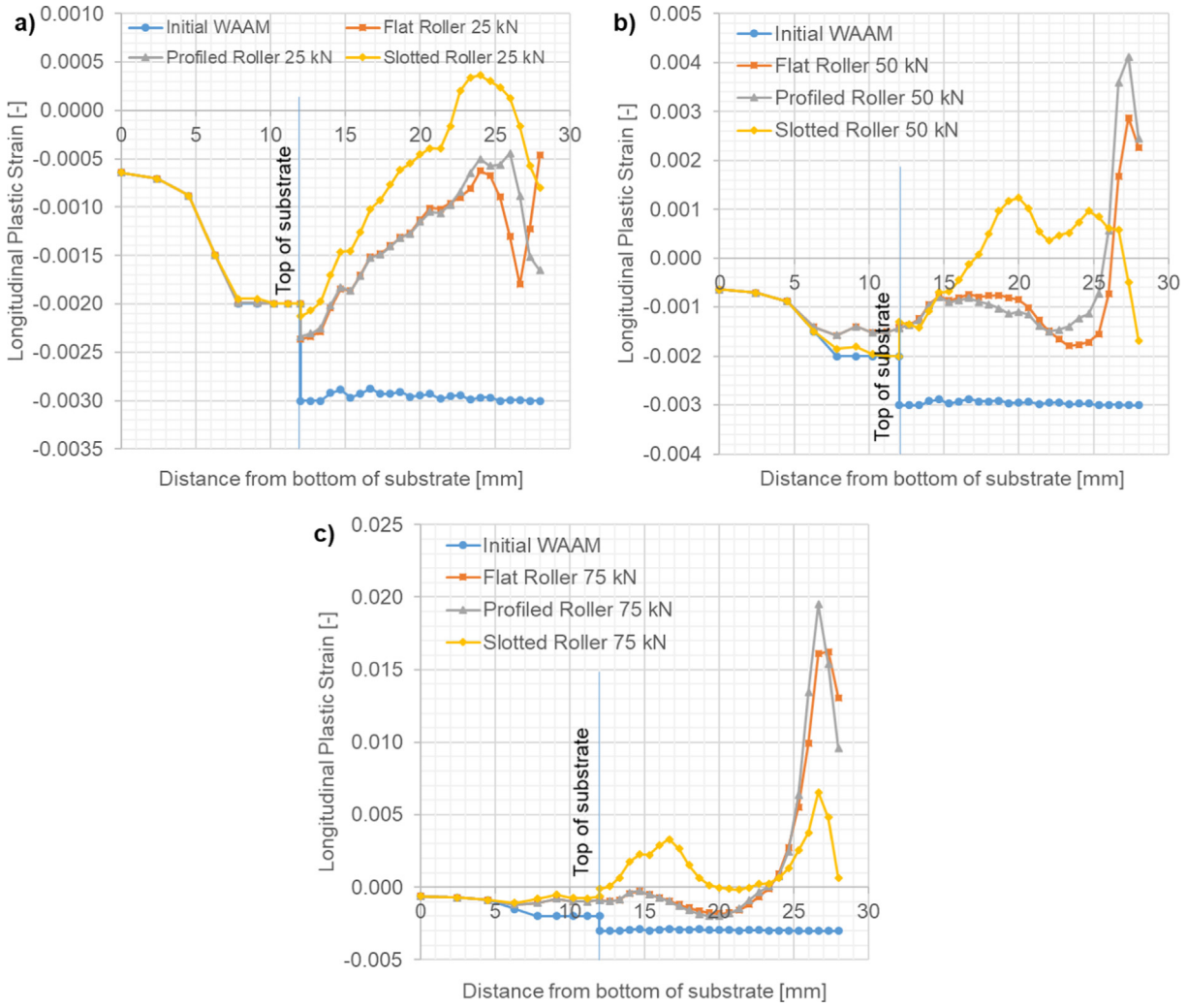

Fig. 16. Influence of roller design on mitigation of the compressive longitudinal PS caused by WAAM deposition. The rolling loads are a) 25 kN, b) 50 kN and c) 75 kN (μ = 0.1).

37.1 kN after WAAM deposition to 2.1 kN after the rolling with the flat roller (F = 50 kN, μ = 0.1). When the clamps were removed, the equilibrium between the tensile and compressive RSs reached shortly with minor redistribution of RS. As a result, the net bending moment was close to zero and the rolled WAAM component remained virtually undistorted, as shown in Fig. 20.

Fig. 21 shows the comparison of vertical distortion after the clamps removal in the long WAAM component rolled with flat, profiled and slotted rollers at rolling loads from 25 kN to 75 kN. In general, the post-build rolling virtually eliminated the distortion caused by the thermal deposition process with all types of investigated rollers and at all rolling loads. The predicted distortion varies from 560 μm for flat roller at F = 25 kN to 0.008 μm for flat roller at F = 75 kN. The flat and profiled rollers are less effective to reduce distortion than the slotted roller at the rolling load of 25 kN. However, the flat and profiled rollers at the rolling loads of 50 kN and 75 kN reduced distortion more effectively than the slotted roller, since the latter caused greater inverse distortion. This is because excessive material was subjected to compressive RS in the WAAM wall after the rolling by the slotted roller (Fig. 15c). It should be reiterated that the predicted distortion in the rolled wall with different rollers (Fig. 21) is all much smaller than the distortion in the as-built wall (Fig. 20).

Given the efficacy of the post-build rolling in mitigation of distortion, the practical implementation of post-build rolling has wide potentials to achieve the required reduction of distortion using slotted roller at lower rolling load or using flat and profiled rollers at higher rolling loads.

3.5. Effect of initial WAAM deposition condition on PS and RS distributions for various rolling loads

Fig. 22 shows the comparison of PS and RS distributions predicted by the flat roller model at various rolling loads with and without consideration of WAAM deposition. The initial WAAM deposition condition plays an important role in the prediction of PS distribution for all the rolling loads. The models without the initial WAAM condition underpredicted the compressive PS in the final state. In contrast, the effect of WAAM deposition on the RS prediction depends on the rolling load. At relatively low rolling load (25 kN) the model without initial WAAM condition underpredicted the tensile RSs that are 7 mm below the rolled surface and in the substrate. With increase of rolling load to 50 kN, the discrepancy between the RSs predicted by the models with and without initial WAAM condition reduced, and at the rolling load of 75 kN, minor difference was found, which can be attributed to the dominant influence of the high pressure rolling over WAAM deposition on the final RS in the wall. However, all the rolling models without initial WAAM condition underpredicted tensile RS in the substrate. These findings partially agree with the result of the numerical

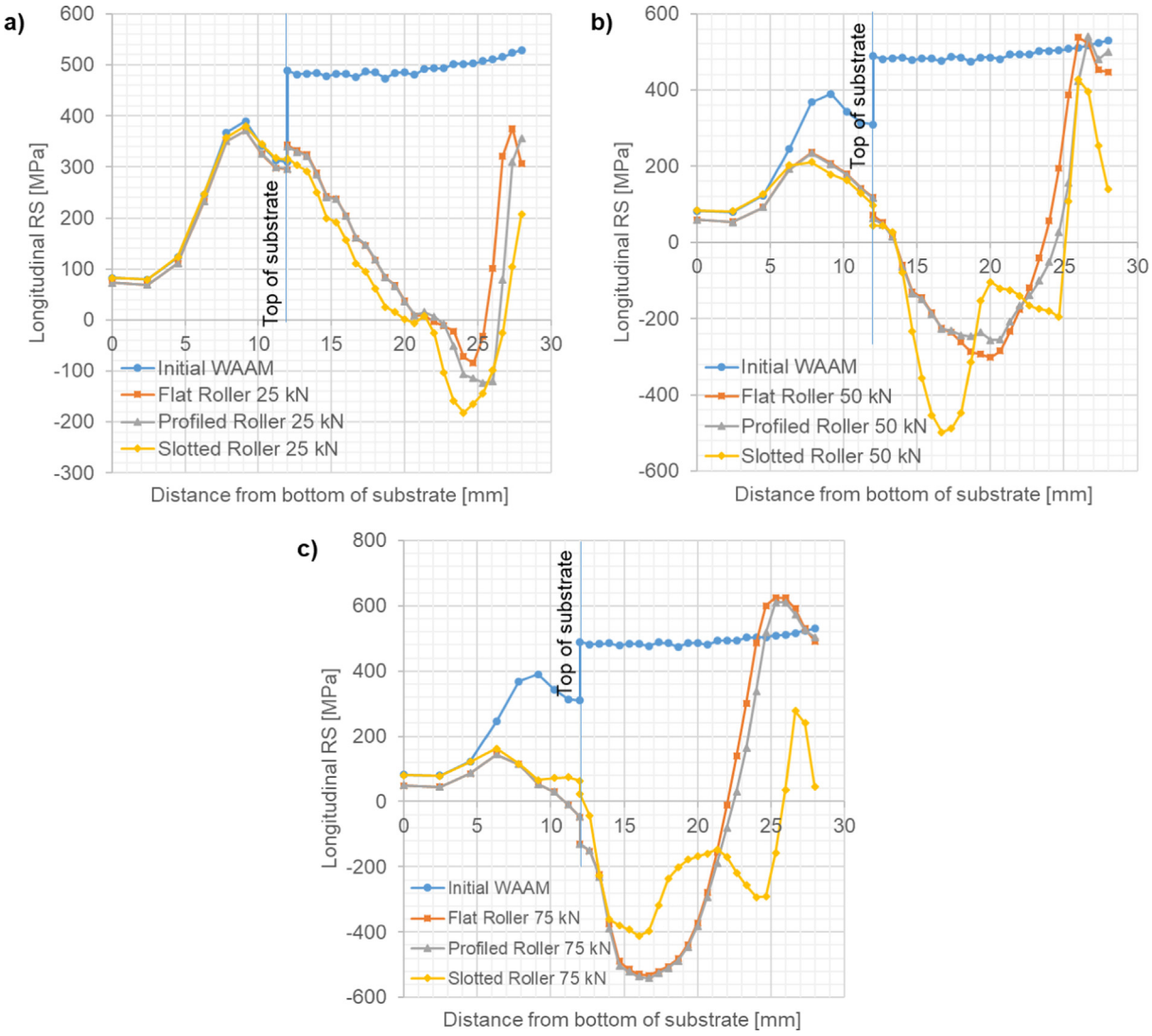

Fig. 17. Influence of roller design on mitigation of the tensile longitudinal RS caused by WAAM deposition. The rolling loads are a) 25 kN, b) 50 kN, and c) 75 kN (μ = 0.1).

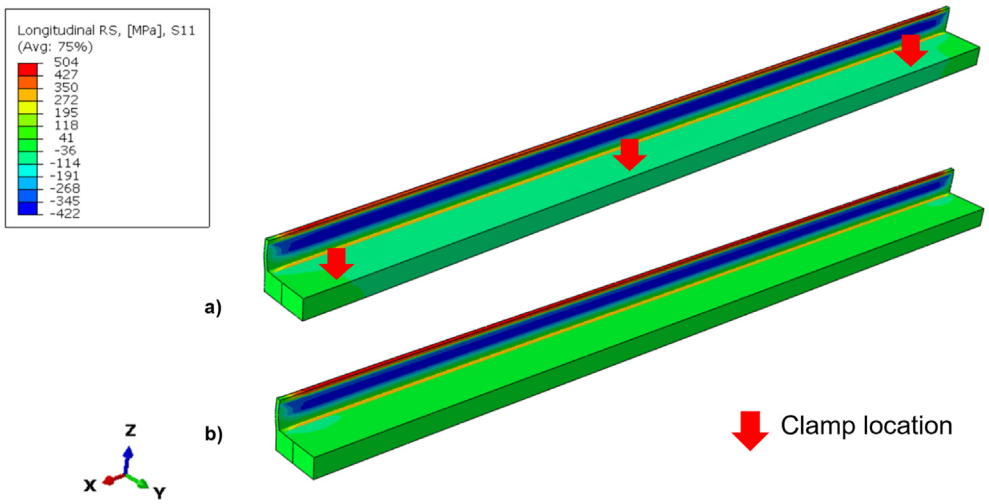

Fig. 18. Longitudinal RS distribution and deformed configuration of the 500 mm long post-build rolled WAAM component a) before and b) after removal of clamps (a deformation scale factor of 25 is used to aid visualisation). Note that the steady-state solution was mapped from the short model with the flat roller (F = 50 kN and μ = 0.1). Red arrows indicate locations of clamps. (For interpretation of the references to colour in this figure legend, the reader is referred to the web version of this article.)

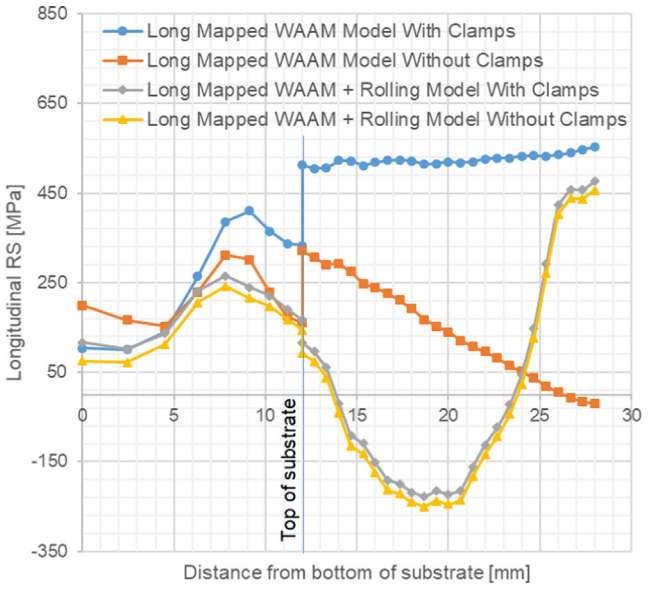

Fig. 19. Influence of the post-build rolling with the flat roller on the WAAM deposition RS obtained by the long mechanical model before and after removal of clamps (F = 50 kN and μ = 0.1).

study by Abbaszadeh et al. [25], who found that at rolling loads larger than 20 kN the difference between the peak RS in the wall, as predicted by the models with and without initial WAAM condition (i.e., initial RS), tends to be negligible. However, Abbaszadeh et al. [25] did not consider the initial PS in their rolling model and claimed that the initially specified RS does not affect distribution of final PS. By contrast, the current study demonstrated the importance of considering the initial WAAM PS in the rolling model to examine the effect of rolling on the final PS.

3.6. Advantages and limitations of post-build rolling for mitigation of RS and distortion in WAAM components

The post-build rolling is a time-saving and cost-effective method to mitigate WAAM-induced RS and distortion, as compared to inter-layer rolling and other RS mitigation techniques. However, it has following limitations. First, the post-build rolling may not be adequately effective for RS mitigation in WAAM walls taller than the wall studied here (e.g., refer to [27] for rolling effect on WAAM RS in a 20-layer 40-mm tall wall). Second, the required rise of the rolling load to increase process effectiveness for the tall wall could cause excessive deformation or even plastic collapse of the wall. Third, the produced RS profile at higher rolling loads could be unfavourable in terms of fatigue performance of the component (i.e., the large region affected by high tensile RS at the rolled surface, as shown in Figs. 5 and 14, can have detrimental effect [45]). Nevertheless, properly designed post-build rolling could be an efficient alternative to the time consuming and complicated inter-layer rolling. Optimisation of in-process rolling through WAAM + Rolling simulations could also be an interesting topic for future work.

4. Conclusions

This modelling study investigated post-build rolling as an efficient method for mitigation of RS and distortion in a WAAM-built steel wall component. The influences of the roller design (flat, profiled and slotted rollers), rolling load (25–75 kN) and roller-to-wall friction coefficient (0–0.8) on the WAAM-induced PS, RS and distortion were examined. The following conclusions are drawn:

1. Post-build rolling can introduce adequate longitudinal tensile PS in the considered wall, thereby counteracting the longitudinal compressive PS and tensile RS generated by the WAAM deposition. For a taller wall, it is anticipated that higher rolling load is required to achieve the similar effectiveness.
2. Post-build rolling with high rolling load is recommended for most effective mitigation of tensile RS. When increasing the rolling load, larger volume of material is deformed with tensile PS, and the WAAM-generated tensile RS converts to compressive RS, which extends deeper in the core of the wall. However, excessive reduction in wall height and potential wall collapse can occur when the rolling load is too high.
3. For all the considered rolling loads, compared to the flat and profiled rollers, the slotted roller induces longitudinal tensile PS with larger extent, and hence it reduces the tensile RS in the wall more effectively.
4. Post-build rolling is effective to mitigate distortion in the WAAM component after removal of clamps. Slotted roller is most effective at a rolling load of 25 kN, but it generates inverse distortion (small magnitude) at rolling loads of 50 kN and 75 kN, due to extensive compressive RS induced by the rolling. With increase of rolling load, the distortion is more markedly reduced for the flat and profiled rollers, but the magnitude of inverse distortion increases for the slotted roller.
5. The efficacy of the flat and profiled rollers is insensitive to the roller-to-wall friction coefficient. In contrast, an increase of friction coefficient drastically increases the efficacy of the slotted roller. The additional friction on the slot is helpful for the slotted roller to penetrate deeper and induce more extensive tensile PS in the wall, but it also increases the horizonal motion resistance.
6. For further simplification of rolling model, the flat roller with a friction coefficient of 0.5 or higher value can be used to represent the profiled roller. The initial condition accounting for

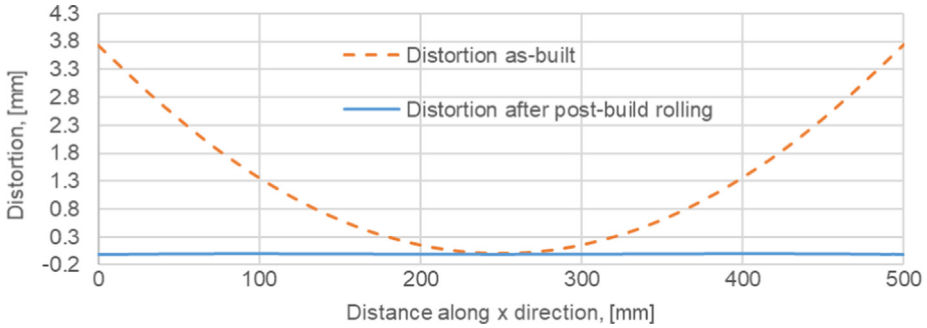

Fig. 20. Comparison of vertical distortion in as-built and rolled full-length WAAM component after removal of clamps (flat roller, F = 50 kN and μ = 0.1).

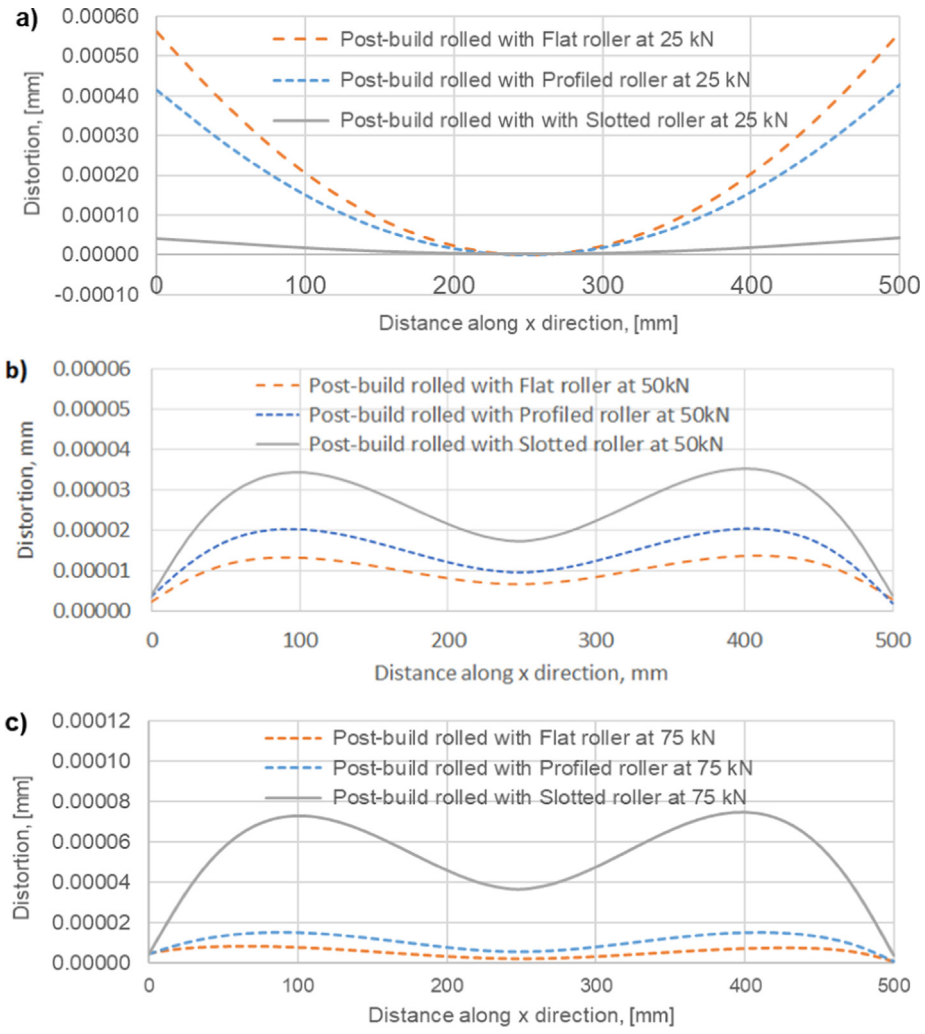

Fig. 21. Comparison of vertical distortion in long WAAM components after removal of clamps for post-build rolling with flat, profiled and slotted rollers at rolling loads of a) 25 kN, b) 50 kN, and c) 75 kN (μ = 0.1).

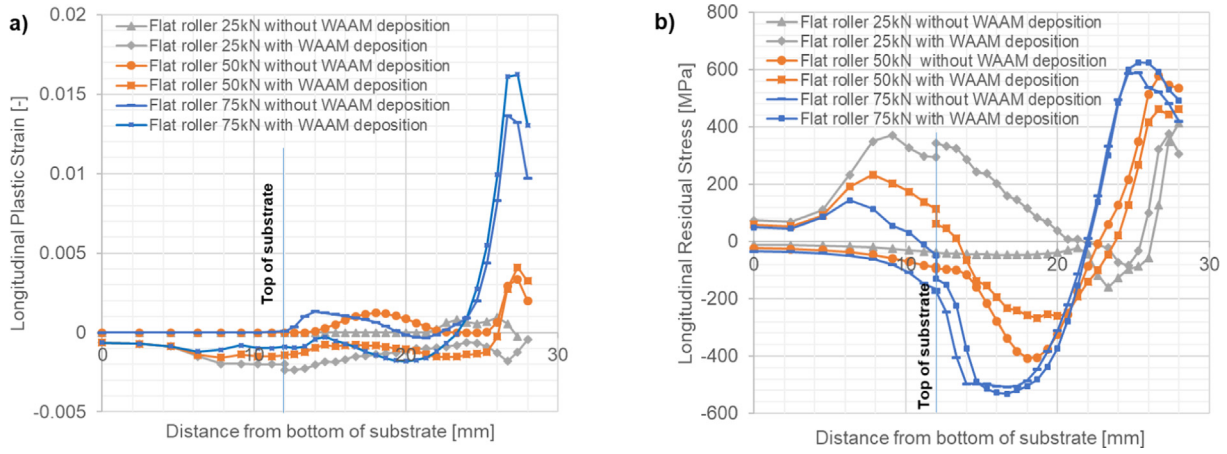

Fig. 22. Comparison of a) PS and b) RS predictions between flat roller models with and without consideration of the WAAM deposition before rolling simulation (μ = 0.5).

the WAAM-induced PS and RS plays significant roles in the predictions of final PS and RS by the rolling model for relatively low rolling load. At high rolling loads, the rolling dominates the final RS in the wall and hence the initial condition has less impact.

CRediT authorship contribution statement

Valeriy Gornyakov: Conceptualization, Methodology, Software, Formal analysis, Investigation, Data curation, Writing – original draft, Visualization. **Jialuo Ding:** Conceptualization, Resources,

Writing – review & editing, Supervision, Project administration. **Yongle Sun:** Conceptualization, Formal analysis, Investigation, Resources, Writing – review & editing, Supervision. **Stewart Williams:** Conceptualization, Resources, Supervision, Project administration.

Declaration of Competing Interest

The authors declare that they have no known competing financial interests or personal relationships that could have appeared to influence the work reported in this paper.

Acknowledgements

Initial stage of this research was guided and supported by Paul Colegrove. Part of this research was technically supported by Daniel Cozzolino, Filomeno Martina and Matyas Benke. The first author thanks Stephan Egerland for the help with English writing. The support by NEWAM (EPSRC grant EP/R027218/1) and WAAM-Mat is also gratefully acknowledged.

Data Availability Statement

Data underlying this study can be accessed through the Cranfield University repository at https://doi.org/10.17862/cranfield.rd.15060285.

References

[1] T.A. Rodrigues, V. Duarte, R.M. Miranda, T.G. Santos, J.P. Oliveira, Current status and perspectives on wire and arc additive manufacturing (WAAM), Materials. 12 (7) (2019) 112, https://doi.org/10.3390/ma12071121.
[2] P.A. Colegrove, H.E. Coules, J. Fairman, F. Martina, T. Kashoob, H. Mamash, et al., Microstructure and residual stress improvement in wire and arc additively manufactured parts through high-pressure rolling, J. Mater. Process. Technol. 213 (10) (2013) 1782–1791, https://doi.org/10.1016/j.jmatprotec.2013.04.012.
[3] Welding Engineering and Laser Processing Centre of Cranfield University, Demo parts built for industry partners. WAAM. Available at: https://waammat.com/about/demo-parts (Accessed: 15 December 2020).
[4] E. Karayel, Y. Bozkurt, Additive manufacturing method and different welding applications, J. Mater. Res. Technol. 9 (5) (2020) 11424–11438, https://doi.org/10.1016/j.jmrt.2020.08.039.
[5] W. Jin, C. Zhang, S. Jin, Y. Tian, D. Wellmann, W. Liu, Wire arc additive manufacturing of stainless steels: a review, Appl. Sci. 10 (5) (2020), https://doi.org/10.3390/app10051563.
[6] J. Gu, J. Ding, S.W. Williams, H. Gu, P. Ma, Y. Zhai, The effect of inter-layer cold working and post-deposition heat treatment on porosity in additively manufactured aluminum alloys, J. Mater. Process. Technol. 230 (2016) 26–34, https://doi.org/10.1016/j.jmatprotec.2015.11.006.
[7] F. Martina, M.J. Roy, B.A. Szost, S. Terzi, P.A. Colegrove, S.W. Williams, J. Meyer, M. Hofmann, Residual stress of as-deposited and rolled wire+arc additive manufacturing Ti–6Al–4V components, Mater. Sci. Technol. 32 (14) (2016) 1439–1448, https://doi.org/10.1080/02670836.2016.1142704.
[8] Z. Lin, K. Song, X. Yu, A review on wire and arc additive manufacturing of titanium alloy, J. Manuf. Processes 70 (2021) 24–45, https://doi.org/10.1016/j.jmapro.2021.08.018.
[9] G. Asala, A.K. Khan, J. Andersson, O.A. Ojo, Microstructural analyses of ATI 718Plus® produced by wire-ARC additive manufacturing process, Metall. Mater. Trans. A. 48 (9) (2017) 4211–4228, https://doi.org/10.1007/s11661-017-4162-2.
[10] G. Marinelli, F. Martina, S. Ganguly, S. Williams, Grain refinement in an unalloyed tantalum structure by combining Wire+Arc additive manufacturing and vertical cold rolling, Additive Manuf. 32 (2020) 101009, https://doi.org/10.1016/j.addma.2019.101009.
[11] G. Marinelli, F. Martina, S. Ganguly, S. Williams, Development of Wire + Arc additive manufacture for the production of large-scale unalloyed tungsten components, Int. J. Refract. Met. Hard Mater. 82 (2019) 329–335, https://doi.org/10.1016/j.ijrmhm.2019.05.009.
[12] S.W. Williams, F. Martina, A.C. Addison, J. Ding, G. Pardal, P. Colegrove, Wire + arc additive manufacturing, Mater. Sci. Technol. 32 (7) (2016) 641–647, https://doi.org/10.1179/1743284715Y.0000000073.
[13] J. Ding, P. Colegrove, J. Mehnen, S. Williams, F. Wang, P.S. Almeida, A computationally efficient finite element model of wire and arc additive manufacture, Int. J. Adv. Manuf. Technol. 70 (2014) 227–236, https://doi.org/10.1007/s00170-013-5261-x.
[14] G.A. Webster, A.N. Ezeilo, Residual stress distributions and their influence on fatigue lifetimes, Int. J. Fatigue 23 (2001) 375–383, https://doi.org/10.1016/S0142-1123(01)00133-5.
[15] P. Dong, F.W. Brust, Welding residual stresses and effects on fracture in pressure vessel and piping components: a millennium review and beyond, J. Press. Vessel Technol. 122 (3) (2000) 329–338, https://doi.org/10.1115/1.556189.
[16] P. Dong, Residual stresses and distortions in welded structures: a perspective for engineering applications, Sci. Technol. Weld. Join. 10 (4) (2005) 389–398, https://doi.org/10.1179/174329305X29465.
[17] J.R. Cho, B.Y. Lee, Y.H. Moon, C.J. Van Tyne, Investigation of residual stress and post weld heat treatment of multi-pass welds by finite element method and experiments, J. Mater. Process. Technol. 155–156 (2004) 1690–1695, https://doi.org/10.1016/j.jmatprotec.2004.04.325.
[18] J. Altenkirch, A. Steuwer, P.J. Withers, S.W. Williams, M. Poad, S.W. Wen, Residual stress engineering in friction stir welds by roller tensioning, Sci. Technol. Weld. Join. 14 (2) (2009) 185–192, https://doi.org/10.1179/136217108X388624.
[19] S.A. Kurkin, V.I. Anufriev, E.S. Milekhin, Improving the mechanical properties of welded joints in the AMg6 alloy by plastic deformation during arc welding, Svar. Proizvod. 27 (1980) 20–24.
[20] J. Sule, S. Ganguly, H. Coules, T. Pirling, Application of local mechanical tensioning and laser processing to refine microstructure and modify residual stress state of a multi-pass 304L austenitic steels welds, J. Manuf. Process. 18 (2015) 141–150, https://doi.org/10.1016/j.jmapro.2015.03.003.
[21] P.A. Colegrove, F. Martina, M.J. Roy, B.A. Szost, S. Terzi, S.W. Williams, P.J. Withers, D. Jarvis, High pressure interpass rolling of Wire + Arc Additively Manufactured titanium components, Adv. Mater. Res. 996 (2014) 694–700, https://doi.org/10.4028/www.scientific.net/AMR.996.694.
[22] J.R. Hönnige, P.A. Colegrove, B. Ahmad, M.E. Fitzpatrick, S. Ganguly, T.L. Lee, et al., Residual stress and texture control in Ti-6Al-4V wire + arc additively manufactured intersections by stress relief and rolling, Mater. Des. 150 (2018) 193–205, https://doi.org/10.1016/j.matdes.2018.03.065.
[23] L.D. Cozzolino, H.E. Coules, P.A. Colegrove, S. Wen, Investigation of post-weld rolling methods to reduce residual stress and distortion, J. Mater. Process. Technol. 247 (2017) 243–256, https://doi.org/10.1016/j.jmatprotec.2017.04.018.
[24] L.D. Cozzolino, Finite element analysis of localised rolling to reduce residual stress and distortion (PhD Thesis), Cranfield University, 2013.
[25] M. Abbaszadeh, J.R. Hönnige, F. Martina, L. Neto, N. Kashaev, P. Colegrove, S. Williams, B. Klusemann, Numerical investigation of the effect of rolling on the localized stress and strain induction for Wire + Arc Additive Manufactured structures, J. Mater. Eng. Perf. 28 (8) (2019) 4931–4942, https://doi.org/10.1007/s11665-019-04249-y.
[26] R. Tangestani, G.H. Farrahi, M. Shishegar, B.P. Aghchehkandi, S. Ganguly, A. Mehmanparast, Effects of vertical and pinch rolling on residual stress distributions in wire and arc additively manufactured components, J. Mater. Eng. Perf. 29 (4) (2020) 2073–2084, https://doi.org/10.1007/s11665-020-04767-0.
[27] V. Gornyakov, Y. Sun, J. Ding, S. Williams, Efficient determination and evaluation of steady-state thermal-mechanical variables generated by wire arc additive manufacturing and high pressure rolling, Model. Simul. Mater. Sci. Eng. (2021), https://doi.org/10.1088/1361-651X/ac35b8 (Accessed: 5 November 2021).
[28] J. Perenda, J. Trajkovski, A. Žerovnik, I. Prebil, Residual stresses after deep rolling of a torsion bar made from high strength steel, J. Mater. Process. Technol. 218 (2015) 89–98, https://doi.org/10.1016/j.jmatprotec.2014.11.042.
[29] J. Lan, S. Feng, L. Hua, The residual stress of the cold rolled bearing race, Procedia Eng. 207 (2017) 1254–1259, https://doi.org/10.1016/j.proeng.2017.10.879.
[30] R. Pan, T. Pirling, J. Zheng, J. Lin, C.M. Davies, Quantification of thermal residual stresses relaxation in AA7xxx aluminium alloy through cold rolling, J. Mater. Process. Technol. 264 (2019) 454–468, https://doi.org/10.1016/j.jmatprotec.2018.09.034.
[31] T.A. Stolarski, S. Tobe, Rolling Contacts, John Wiley & Sons, Ltd, Chichester, UK, 2000. Available at: DOI:10.1002/9781118903001 (Accessed: 23 April 2020).
[32] H.E. Coules, G.C.M. Horne, S. Kabra, P. Colegrove, D.J. Smith, Three-dimensional mapping of the residual stress field in a locally rolled aluminium alloy specimen, J. Manuf. Process. 26 (2017) 240–251, https://doi.org/10.1016/j.jmapro.2017.02.010.
[33] I.M. Hutchings, P. Shipway, Tribology: Friction and Wear of Engineering Materials, second ed., Elsevier Ltd., 2017.
[34] L.S. Marks, Marks' standard handbook for mechanical engineers, eleventh edition, [90. anniversary edition]. E.A. Avallone, T. Baumeister, A.M. Sadegh (Eds.), McGraw-Hill, New York, 2007.
[35] V. Gornyakov, Y. Sun, J. Ding, S. Williams, Computationally efficient models of high pressure rolling for wire arc additively manufactured components, Appl. Sci. 11 (1) (2021) 402, https://doi.org/10.3390/app11010402.
[36] M.A. Thompson, M. Fresini, J. DosSantos, J. Hedgegard, I.M. Richardson, Improving the competitiveness of the European steel fabrication industry using synchronised tandem wire welding technology [Technical]. SYNFAB, 2005. Report No.: 3.
[37] C.V. Haden, G. Zeng, F.M. Carter, C. Ruhl, B.A. Krick, D.G. Harlow, Wire and arc additive manufactured steel: tensile and wear properties, Additive Manuf. 16 (2017) 115–123, https://doi.org/10.1016/j.addma.2017.05.010.

[38] P. Colegrove, C. Ikeagu, A. Thistlethwaite, S. Williams, T. Nagy, W. Suder, A. Steuwer, T. Pirling, Welding process impact on residual stress and distortion, Sci. Technol. Weld. Join. 14 (8) (2009) 717–725, https://doi.org/10.1179/136217109X406938.
[39] W. Woo, G.B. An, E.J. Kingston, A.T. DeWald, D.J. Smith, M.R. Hill, Through-thickness distributions of residual stresses in two extreme heat-input thick welds: a neutron diffraction, contour method and deep hole drilling study, Acta Mater. 61 (10) (2013) 3564–3574, https://doi.org/10.1016/j.actamat.2013.02.034.
[40] J.R. Hönnige, P.A. Colegrove, S. Ganguly, E. Eimer, S. Kabra, S. Williams, Control of residual stress and distortion in aluminium wire + arc additive manufacture with rolling, Additive Manuf. 22 (2018) 775–783, https://doi.org/10.1016/j.addma.2018.06.015.
[41] M. Cook, E.C. Larke, Resistance of copper and copper alloys to homogeneous deformation in compression, J. Inst. Met. 71 (January 1945) 371–390.
[42] H.E. Coules, P. Colegrove, L.D. Cozzolino, S.W. Wen, J.F. Kelleher, High pressure rolling of low carbon steel weld seams: Part 2 – Roller geometry and residual stress, Sci. Technol. Weld. Join. 18 (1) (2013) 84–90, https://doi.org/10.1179/1362171812Y.0000000080.
[43] A.R. McAndrew, Rosales M. Alvarez, P.A. Colegrove, J.R. Hönnige, A. Ho, R. Fayolle, K. Eyitayo, I. Stan, P. Sukrongpang, A. Crochemore, Z. Pinter, Interpass rolling of Ti-6Al-4V wire + arc additively manufactured features for microstructural refinement, Additive Manuf. 21 (2018) 340–349, https://doi.org/10.1016/j.addma.2018.03.006.
[44] S.M. Hassani-Gangaraj, M. Carboni, M. Guagliano, Finite element approach toward an advanced understanding of deep rolling induced residual stresses, and an application to railway axles, Mater. Des. 83 (2015) 689–703, https://doi.org/10.1016/j.matdes.2015.06.026.
[45] R.C. McClung, A literature survey on the stability and significance of residual stresses during fatigue, Fatigue Fract. Eng. Mater. Struct. 30 (3) (2007) 173–205, https://doi.org/10.1111/j.1460-2695.2007.01102.x.

2021-12-21

Understanding and designing post-build rolling for mitigation of residual stress and distortion in wire arc additively manufactured components

Gornyakov, Valeriy

Elsevier

Gornyakov V, Ding J, Sun Y, Williams S. (2022) Understanding and designing post-build rolling for mitigation of residual stress and distortion in wire arc additively manufactured components. Materials and Design, Volume 213, January 2022, Article number 110335

https://doi.org/10.1016/j.matdes.2021.110335